Friction in surface micromachined microengines[*]

S. L. Miller, J. J. Sniegowski, G. LaVigne, and P. J. McWhorter

Sandia National Laboratories
Mail Stop 1080
P.O. Box 5800
Albuquerque, NM 87185-1080

Abstract

Understanding the frictional properties of advanced Micro-Electro-Mechanical Systems (MEMS) is essential in order to develop optimized designs and fabrication processes, as well as to qualify devices for commercial applications. We develop and demonstrate a method to experimentally measure the forces associated with sliding friction of devices rotating on a hub. The method is demonstrated on the rotating output gear of the microengine recently developed at Sandia National Laboratories. *In-situ* measurements of an engine running at 18300 rpm give a coefficient of friction of 0.5 for radial (normal) forces less than 4 µN. For larger forces the effective coefficient of friction abruptly increases, suggesting a fundamental change in the basic nature of the interaction between the gear and hub. The experimental approach we have developed to measure the frictional forces associated with the microengine is generically applicable to other MEMS devices.

1. Introduction

Friction is a relatively uncharacterized property of Micro-Electro-Mechanical Systems (MEMS) that can significantly impact both their performance and reliability. Frictional effects include both increasing the power requirements of MEMS actuators and, more significantly, inducing wear that can result in premature device failure. Friction can also impact the dynamical behavior of MEMS, resulting in undesirable modes of operation if drive signals are not properly engineered. Consequently, a basic understanding of frictional effects in MEMS is essential for them to receive widespread acceptance in commercial applications, where performance and reliability must both be optimized and quantified.

Friction-related research in the area of rotating MEMS structures has been limited primarily to two types of structures. Rolling friction has been examined in harmonic side-drive motors,[1,2] often termed wobble motors. Sliding friction that occurs between a rotating disk and supporting hub has been examined for electrostatic motors where the stators completely encircle the rotor.[3,4] These particular rotating devices are not capable of delivering torque to an external load. A technologically important device that exhibits sliding friction and that is capable of driving external loads is the microengine recently developed at Sandia National Laboratories.[5,6,7]
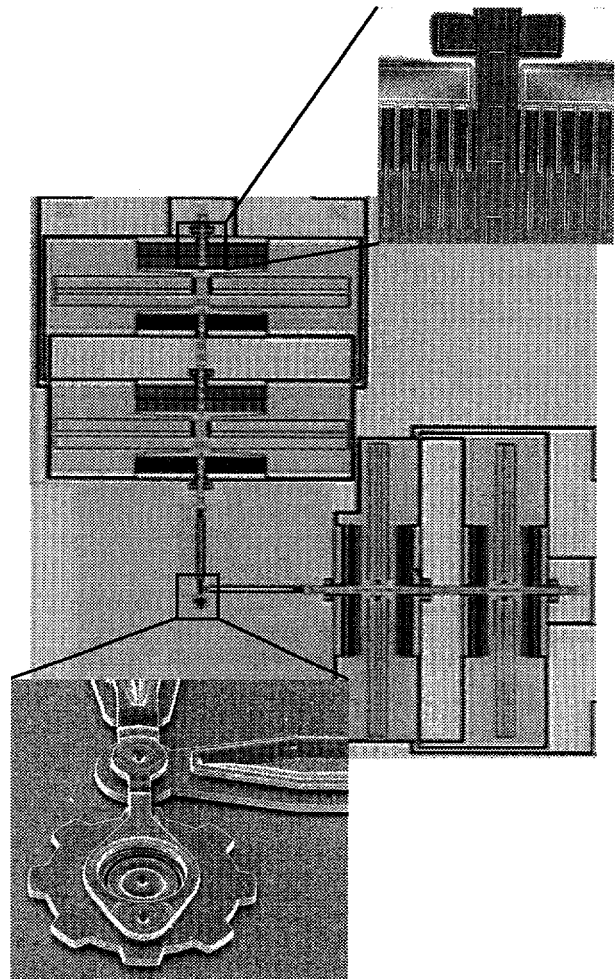

Fig. 1. The microengine consists of orthogonally oriented linear comb drive actuators mechanically connected to a rotating gear capable of providing torque to a load device.

The microengine (Fig. 1) consists of linear electrostatic actuators that are mechanically coupled to an output gear. The electrostatic combs permit the application of attractive forces in four directions. The resulting forces are transmitted to the gear through mechanical linkages in a way that results in continuous rotation of the output gear. The moveable comb structures are mechanically supported by springs, which are attached to the substrate. A complete description of the technology used to fabricate the microengine is given elsewhere,[7] as is additional design information.[6] The microengine has been operated at speeds in excess of 300,000 rpm, with a current endurance record of 3,200,000,000 revolutions accrued on a single engine.

In this paper, we develop an *in-situ* method to measure frictional forces between the rotating output gear and hub of the microengine. To do this, we model the dynamics of the engine, and experimentally determine the basic physical parameters of the structure, such as the spring constant, electrostatic force constant, and damping coefficient. The experimentally measured values are compared with those theoretically expected. As a further check of the dynamical model, theoretical predictions of the engine response are experimentally verified. Finally, frictional forces are determined from measurements of operating engines. While the details of the method presented in this paper are specific to the microengine device, the approach used to measure and characterize friction is generically applicable to a wide range of MEMS devices.

2. Friction Measurement Model

Our objective is to determine experimentally the radial (normal) force between the output gear and the hub on which it rotates, and the resulting tangential frictional force. Ideally, these forces should be determined from experimentally measured quantities obtained from an engine during normal operation. Such an *in-situ* measurement technique would permit the determination of how different operational parameters impact friction, such as accrued number of cycles, loading conditions, drive signals, lubricants, temperature, etc. An additional requirement of the measurement approach is that it must be possible to determine the necessary physical parameters directly from a set of measurements independent from those used to determine the frictional forces. These objectives are met by our approach, as described below.

Several forces must be considered when modeling the dynamics of the microengine (see Fig. 2). The
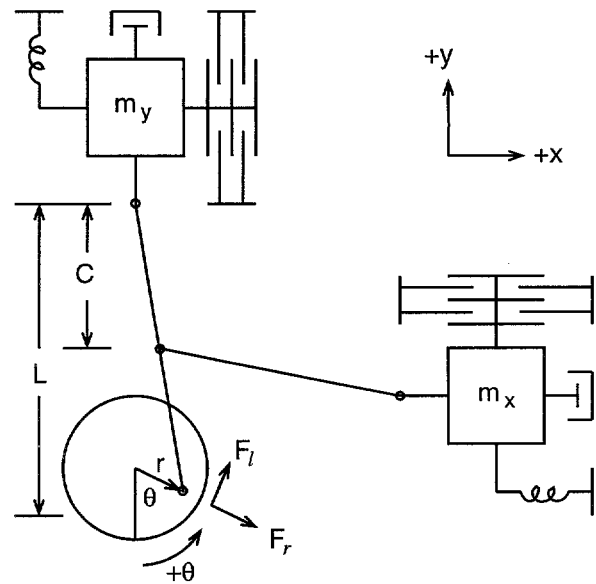

Fig. 2. The comb drives experience forces due to supporting springs, air damping, electrostatic attraction, and the mechanical linkages connecting them to the gear.

electrostatic forces resulting from voltages applied to the comb drives, which are always attractive, are given by

$$F_x = \pm a_x V_x^2 \tag{1}$$

$$F_y = \pm a_y V_y^2, \tag{2}$$

where the positive signs are used when combs are pulling in the positive directions, and similarly for the negative signs. The term a, called the electrostatic force constant, is related to geometrical quantities by[7]

$$a = n\varepsilon\frac{h}{g}, \tag{3}$$

where n is the number of fingers in the comb drive, ε is the dielectric constant of the material between the interdigitated fingers, h is the comb thickness, and g is the width of the gap.

The springs supporting the combs provide a restoring force given by

$$F_x = -k_x x \tag{4}$$

$$F_y = -k_y y. \tag{5}$$

The spring constants k are related to Young's modulus E, for the present design, by[8]

$$k = 4Eh\left(\frac{w}{L}\right)^3, \tag{6}$$

where h is the spring thickness, w is the width of the spring beams, and L is the length of the spring.

DISCLAIMER

**Portions of this document may be illegible
in electronic image products. Images are
produced from the best available original
document.**

When operating in air, the moving comb structures can experience resistive forces due to air damping, which are approximated by

$$F_x = -d_x \frac{dx}{dt} \tag{7}$$

$$F_y = -d_y \frac{dy}{dt}, \tag{8}$$

where the terms d_x and d_y are the damping coefficients.

Even though the microengine components have small mass, significant inertial forces can result when the engine is operated at sufficiently high speeds (> 100000 rpm). Thus, we include the linear inertia of the comb drives and linkage arms when solving the dynamical equations of the microengine. The effect of the rotational inertia of the output gear is negligible for the present design.

To simplify the form of the equations, we define the following terms:

$$\delta_x = \frac{d_x}{2m_x} \tag{9}$$

$$\omega_x = \sqrt{\frac{k_x}{m_x}} \tag{10}$$

$$\gamma = \frac{C}{L}, \tag{11}$$

where m_x is the mass of the structure moving in the x direction and C and L are geometrical quantities (see Fig. 2). Omitting the details of the derivation, we solve Newton's equation $\Sigma F = ma$, and obtain

$$\frac{F_r}{kr} = \gamma \frac{\pm a_x}{kr} V_x^2 \sin(\theta) - \frac{\pm a_y}{kr} V_y^2 \cos(\theta) + \cos(\theta) - 1$$

$$+ \sin(\theta)\cos(\theta)\left[\ddot{\theta}\left(\frac{1}{\omega_y^2} - \frac{\gamma^2}{\omega_x^2}\right) + 2\dot{\theta}\left(\frac{\delta_y}{\omega_y^2} - \frac{\gamma^2 \delta_x}{\omega_x^2}\right)\right]$$

$$+ \dot{\theta}^2\left[\frac{\cos^2(\theta)}{\omega_y^2} + \frac{\gamma^2 \sin^2(\theta)}{\omega_x^2}\right] + (1 - \gamma^2)\sin^2(\theta) \tag{12}$$

and

$$\frac{F_l}{kr} = \gamma \frac{\pm a_x}{kr} V_x^2 \cos(\theta) + \frac{\pm a_y}{kr} V_y^2 \sin(\theta) - \sin(\theta)$$

$$- \dot{\theta}^2 \sin(\theta)\cos(\theta)\left(\frac{1}{\omega_y^2} - \frac{\gamma^2}{\omega_x^2}\right) - \frac{\gamma^2 \cos^2(\theta)}{\omega_x^2}(\ddot{\theta} + 2\delta_x \dot{\theta})$$

$$- \frac{\sin^2(\theta)}{\omega_y^2}(\ddot{\theta} + 2\delta_y \dot{\theta}) + (1 - \gamma^2)\sin(\theta)\cos(\theta) \tag{13}$$

where F_r and F_l are the radial and load (tangential) components of the force acting on the gear by the drive arm (see fig. 2). The term r is the radius at which the drive arm connects to the gear, and we let $k = k_x = k_y$. In fact, the design of the present engine is such that $k_x = k_y$, $a_x = a_y$, and $d_x = d_y$. Even so, in some equations the subscripts x and y will be preserved to facilitate physical insight.

The above equations are expressed in a dimensionless form, where the forces are divided by the convenient scale factor kr. The quantity kr is a force whose magnitude is equal to that exerted by the springs when the comb drive is displaced a distance of one radius. Also note the derivation of Eqs. (12) and (13) makes no specific assumptions regarding the drive signals V_x and V_y.

Eqs. (12) and (13) provide a method to experimentally determine the radial and tangential force exerted on the gear by the drive arm at the pin joint. This permits the characterization of friction between the gear and hub, as well as the torque due to a load connected to the gear. To apply the method, certain physical parameters must first be determined experimentally, as described in the following section.

3. Determination of Physical Parameters

3.1. Spring constant and damping coefficient

The spring constant k and damping coefficient d are determined experimentally from measurements of damped free oscillations. When the gear is displaced through some initial angle and then released, it will experience damped oscillations about the equilibrium position of $\theta = 0$. For small amplitude free oscillations, i.e. when the y displacement is small, the normal force between the gear and hub will be small, and the resulting friction will be small relative to the air damping force and comb drive inertial forces. Also, calculations show the inertial forces due to the small output gear are negligible compared to those of the comb drive. Given these approximations, the equation of motion for free oscillations reduces to

$$m_x \ddot{x} + d_x \dot{x} + k_x x = 0. \tag{14}$$

Using the geometrical relationship $x = \gamma r \sin(\theta)$, the solution to Eq. (14) can be expressed as:

$$\theta(t) = \sin^{-1}\left[\sin(\theta_0)\exp(-\delta_x t)\left(\cos(\omega t) + \frac{\delta_x}{\omega}\sin(\omega t)\right)\right] \tag{15}$$

where

$$\omega = \sqrt{\omega_x^2 - \delta_x^2} \qquad (16)$$

and δ_x and ω_x are given by Eqs. (9) and (10).

Experimental measurements of damped free oscillations of the type described above are shown in Fig. 3. The solid line is a fit of Eq. (15) to the data using $\omega = 10900$ rad/sec and $\delta_x = 2300$ sec^{-1}. The good fit supports the assumptions made in the derivation of Eq. (15).

Using Eqs. (10) and (16), the above experimentally measured values result in a spring constant of $k_x = 0.071$ N/m. To perform this calculation, the mass $m_x = 5.7 \times 10^{-10}$ kg was used, which was determined from the known density of polysilicon ($\rho = 2.33$ g/cm^3) and the volume of the structure. The resulting value of Young's modulus, computed using Eq. (6), is $E = 169 \times 10^9$N/m^2. This is comparable to the value given in the literature, which spans $E = \sim140\text{-}160 \times 10^9$N/m^2.[9] The slight difference is either due to our measurements being made on a higher quality polysilicon spring (with a higher value of Young's modulus), or is due to slight errors in the spring geometry, which is amplified by the cubic term in Eq. (6).

3.2. Electrostatic force constant

The value of the electrostatic force constant a (see Eq. (3)) can be measured experimentally from static measurements. If we let $V_x = V_y = V$, and ramp V until $\theta = 90°$, the resulting value of the applied voltage $V_{90°}$ is related to $k_y r/a$ by

$$\frac{k_y r}{a} = (V_{90°})^2. \qquad (17)$$
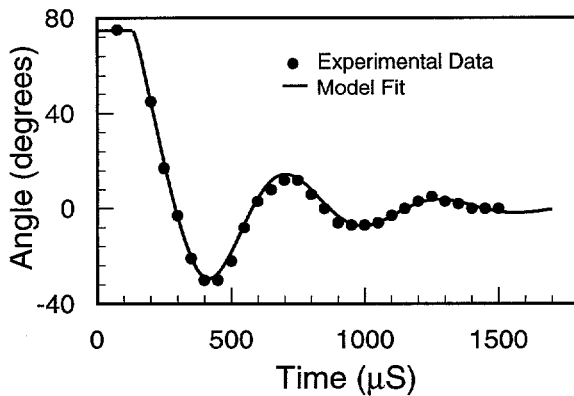
We experimentally obtain a value of $V_{90°} = 46$ V, and

hence $k_y r/a = 2100$ V^2. Using the known value of $r = 17\mu$m and the previously measured value of k_x, we obtain $a = 5.7 \times 10^{-10}$ F/m from Eq. (17). This experimentally determined value is in good agreement with the expected value of $a = 6.0 \times 10^{-10}$ F/m calculated from Eq. (3).

3.3. Experimental verification of model parameters

To verify further the experimentally determined values of the physical parameters, as well as validate the modeling approach, several predictions of the engine behavior were made and experimentally verified. Specifically, the angular position of the gear as a function of the applied voltage V_x and V_y was predicted using the parameters determined above, and then experimentally measured. The static behavior of the engine, when frictional forces are small, is described by

$$0 = \gamma \frac{a}{kr} V_x^2 \cos(\theta) + \frac{a}{kr} V_y^2 \sin(\theta) - \sin(\theta)$$

$$+ (1 - \gamma^2)\sin(\theta)\cos(\theta). \qquad (18)$$

The angular displacement of the engine gear, as predicted by Eq. (18), is shown in Fig. 4 as a function of V_x for several constant values of V_y. The solid lines are the predictions using the previously determined physical parameters, and the dots are the experimentally measured results. The experimental data are in good agreement with the predictions. The deviation at low values of V_x is due to the effects of static friction, which is not explicitly included in Eq. (18).

Fig. 3. The spring constant d and air damping coefficient d are determined by fitting Eq. (15) to experimental data.
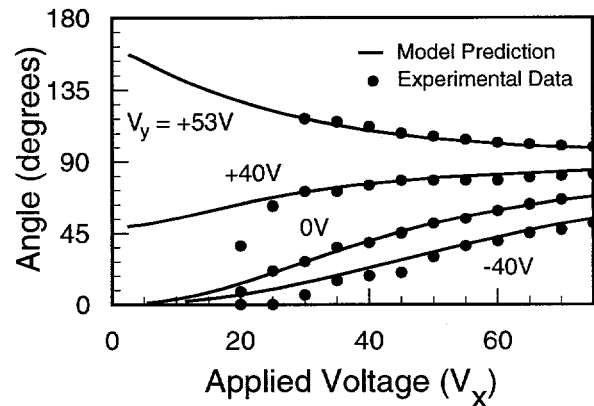
Fig. 4. The accuracy of the physical parameters is validated by the agreement between experimental data and model predictions made using previously determined physical parameters. The deviation at low V_x values is due to static friction, which is not included in Eq. (18).

4. Friction Measurements

4.1. Drive Signals

To apply Eqs. (12) and (13) to determine frictional forces, one must operate the engine with an appropriate set of drive signals $V_x(t)$ and $V_y(t)$, and measure the angular displacement $\theta(t)$. If the drive signals are not appropriately chosen (e.g. square waves or sine waves are used), the angular speed, radial force, and resulting frictional load force can experience large fluctuations during a single period of rotation. When this occurs, the interpretation of the results becomes more difficult. We now consider how to create drive signals where the angular speed of the output gear is approximately constant, without knowing the frictional forces *a-priori*.

The drive signals, angular position, radial force, and load force are all interrelated according to[10]

$$V_x = \pm\left\{\frac{1}{\gamma}\frac{k_x r}{a}\left(\frac{\gamma^2}{\omega_x^2}[(\ddot{\theta} + 2\delta_x\dot{\theta})\cos(\theta) - \dot{\theta}^2\sin(\theta)]\right.\right.$$
$$\left.\left. + \left(\frac{F_r}{k_x r} + \gamma^2\right)\sin(\theta) + \frac{F_l}{k_x r}\cos(\theta)\right)\right\}^{\frac{1}{2}}$$
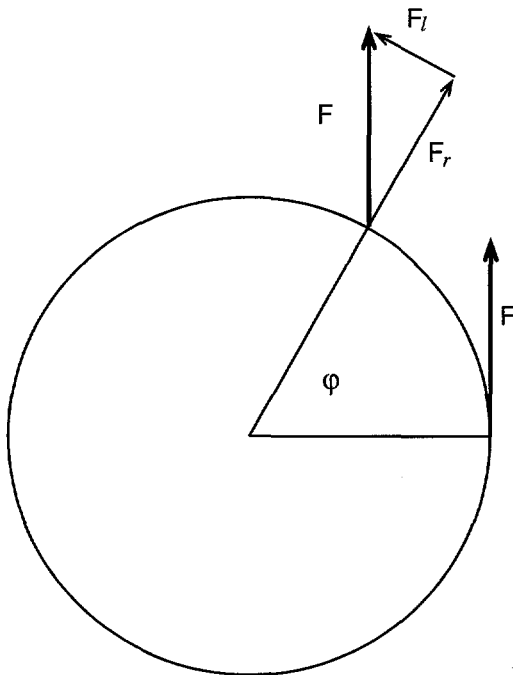
(19)

and

Fig. 5. The output gear of the engine self-adjusts such that the tangential component of the applied force F, referred to as the load force F_l, balances the frictional load torque. If the frictional force varies during rotation, the angle of advancement φ also changes.

$$V_y = \pm\left\{\frac{k_y r}{a}\left(\frac{1}{\omega_x^2}[(\ddot{\theta} + 2\delta_y\dot{\theta})\sin(\theta) + \dot{\theta}^2\cos(\theta)]\right.\right.$$
$$\left.\left. + 1 - \left(\frac{F_r}{k_y r} + 1\right)\cos(\theta) + \frac{F_l}{k_y r}\sin(\theta)\right)\right\}^{\frac{1}{2}}.$$

(20)

Consider the case where drive signals $V_x(t)$ and $V_y(t)$ are created using Eqs. (19) and (20), by setting $\theta(t) = \omega t$,[11] $F_r/kr = 0$, and $F_l/kr = 2$. If the value of the load force term is set large enough to overcome static friction, the engine will rotate when the drive signals are applied. Since the actual forces resulting during operation are typically different from those used in the calculation of the drive signals, the gear dynamically "self-adjusts" so that the force provided by the comb drives properly balances the actual frictional torque.

This dynamical "self-adjusting" becomes intuitive when one examines Fig. 5. Suppose the drive signal results in a force vector of magnitude F at the pin joint of the gear, with the force vector rotating at some constant angular speed ω. If the frictional torque is precisely balanced by F, then the gear will rotate at a speed ω with the force vector being tangential to it. If the magnitude of the frictional torque is smaller, the gear will rotate at an average speed of ω, but at an advanced angle φ. The angle of advancement self adjusts such that the tangential component of F exactly balances the frictional load torque, as shown in Fig. 5. The fact that the frictional force impacts the angle of advancement is the underlying conceptual principle that permits the present friction measurement technique to work.
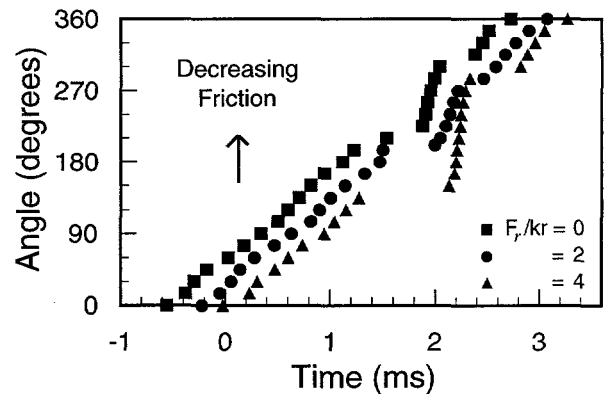

Fig. 6. The experimentally measured angular position of the engine gear is shown for three different drive signals. The angle of advancement spans ~60° for the present drive signals, and is a direct indication of a wide range in frictional load torques.

4.2. Data Acquisition

An engine was operated with a series of six sets of drive signals created by evaluating Eqs. (19) and (20) using $\theta(t) = \omega t$, $\omega = 1917$ rad/sec (18300 rpm), $F_t/kr =$ 1.75, and $F_r/kr = 0$, 1, 2, 2.5, 3, and 4. The other parameters in Eqs. (19) and (20) were determined experimentally, as discussed in the previous section. The angular position θ of the engine output gear was measured using a phase-delayed strobe system; by adjusting the phase of the strobe light relative to that of the periodic drive signal, the angle as a function of time was measured directly.

The results are shown in Fig. 6, where only the three cases $F_r/kr = 0$, 2, and 4 are shown for clarity. Note that in the range $0° < \theta < 180°$ the engine rotates relatively smoothly for each drive signal. Above ~ 180°, the engine experiences a dynamical behavior called lateral clamping.[12] Our friction analysis focuses on the range where lateral clamping does not occur.

Note that the relative phase of the engine angle in Fig. 6 is different for each drive signal. This phase shift is a direct result of the engine experiencing different frictional forces for each drive signal. As the magnitude of the radial force applied to the engine gear decreases, the resulting frictional force decreases, which decreases the torque required to rotate the gear, which causes the gear angle to advance (self-adjust) so the proper torque is actually delivered to the gear. Since the gear "self-adjusts" to the drive signals, the actual forces experienced by the gear are, in general, different than those used in the calculation to create the drive signals. To determine the forces actually experienced by the gear, Eqs. (12) and (13) must be evaluated. In addition to the standard physical constants, all that is required as inputs are the drive signals $V_x(t)$ and $V_y(t)$ used to operate the engine, and the experimentally measured angle $\theta(t)$.

4.3. Analysis

The measured load torque $\tau_l(t)$ applied to the gear is plotted in Fig. 7 as a function of the measured radial force $F_r(t)$ between the gear and hub for a fixed total force. Again referring to Fig. 5, if the frictional force decreases, the gear advances, causing the externally applied radial force to increase and the externally applied torque to decrease. The relationship between the two is what is shown, both theoretically and experimentally, in Fig. 7. Only a single drive signal is considered in this figure. The data points are computed from Eqs. (12) and (13), where the experimentally
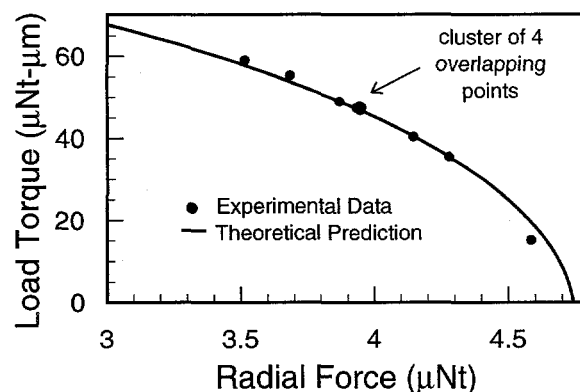

Fig. 7. The theoretical relationship between the load torque and radial force results from the gear "self-adjusting" to varying frictional forces. The experimental data points indicate a distribution of effective coefficients of friction exists.

measured angle and experimentally applied drive signals are used as inputs. The data span a range of forces and torques. The solid line represents the relationship between the radial force and load torque theoretically expected for the drive signals applied to the engine. The actual frictional force is what determines where the points lie scattered along the theoretical curve. If the frictional force changes as the gear rotates, the gear simply self-adjusts to the changing load torque.

Most of the experimental points in Fig. 7 are clustered near one another, with a few outliers. This suggests that there may be a distribution of effective coefficients of friction experienced by the gear as it rotates. The potential ability to experimentally microprobe the distribution of local asperities of a spinning gear will be extensively investigated in future work.

To determine the functional form of the frictional force experienced by the gear, the load torque vs. radial force curves for each of six different drive signals was measured. The results are shown in Fig. 8, where each cluster of data points results from a different drive signal. The data for each drive signal span an arc (the same effect as shown in Fig. 7) indicating a distribution in frictional forces. The value of F_r/kr used to create each drive signal (see Sect. 4.2) is also shown for reference. Recall that the analysis does not depend on how any given drive signal was created.

The conventional coefficient of friction ($F_f = \mu F_n$) is given in terms of the load torque τ_l and radial force F_r by
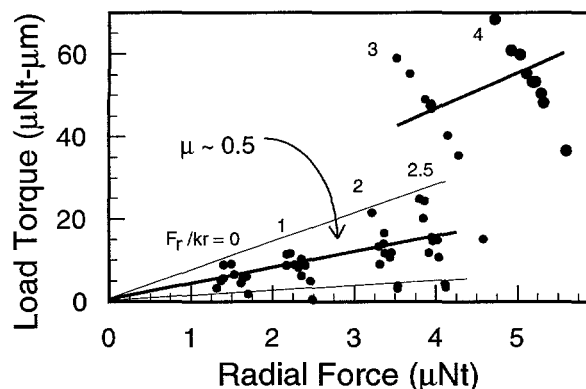
Fig. 8. Conventional friction is experimentally observed for a series of four drive signals that result in low gear forces. For higher applied forces, the nature of friction abruptly changes.

$$\mu = \frac{\tau_l}{r_h F_r}, \tag{21}$$

where r_h is the radius at which the gear contacts the hub (8 μm in the present gear). The straight line through the middle of the first four sets of points also passes through the origin, and results in a coefficient of friction of $\mu \sim$ 0.5. The arched scatter in the data indicate a distribution in values of the coefficient of friction experienced by the gear as it rotates (see Fig. 7). Thus we conclude that conventional friction between the gear and hub occurs for measured radial forces less than ~4 μN (i.e. for the first four sets of data in Fig. 8), and the local frictional force fluctuates as the gear rotates.

For drive signals that result in larger forces, the nature of friction abruptly changes. Still referring to Fig. 8, the experimental data for the final two drive signals lie significantly higher on the load torque vs. radial force arc. The limited data suggest the apparent value of the coefficient of friction is higher, and suggest the y-intercept is non-zero. This unique behavior has not been previously reported.

There are at least two possible explanations for the abrupt change in the frictional behavior of the gear seen in Fig. 8. As the force applied by the comb drives to the gear increases, the gear could torque out of plane with the substrate to such an extent that different surfaces begin to contact and rub. Such a change in the geometrical configuration of the system could give rise to an abrupt force-dependent change in the dynamical behavior of the gear. Another possible explanation is the role that air plays in the frictional dynamics of two curved rubbing surfaces may abruptly change with applied force.[13]

5. Discussion

Though the details of the frictional characterization method are specific to the microengine, some results are generically applicable to a broad range of rotating MEMS devices. Of particular significance is understanding how rotating systems self-adjust to drive signals. This self-adjustment not only results in dynamical fluctuations in the system when frictional forces vary, but can result in huge variations in the forces experienced by the system if the drive signals are not carefully engineered. By appropriately modeling the system, and experimentally measuring the frictional forces, one can create optimized drive signals that result in the desired dynamical behavior, and do so with a minimum of stress and power dissipation. This approach to create engineered drive signals could have a significant impact on both the performance and reliability of many types of MEMS devices.

The method to measure frictional forces has several features that are crucial to its value in characterizing rotating MEMS. The first is the ability to determine experimentally the physical parameters necessary for the friction analysis, and to do so independent of the friction-specific measurements. Decoupling the two types of measurements helps ensure that the friction results have physical significance, rather than being a mathematical artifact of a high-dimensional curve fit, for example. The second essential feature of the method is the ability to determine experimentally the frictional forces during normal engine operation. This permits one to determine how different operational parameters impact friction, such as accrued number of cycles, loading conditions, drive signals, lubricants, temperature, etc. Such results could facilitate the optimization of MEMS designs and processes. They could also facilitate reliability characterization, the development of reliability screening techniques, and reliability enhancement.

The method to measure frictional forces also has the potential for increasing our fundamental understanding of frictional effects in small geometry devices. For example, fluctuations in friction, either in the spatial or temporal domain, potentially can be characterized. The observation of fundamentally new behavior, such as that shown in Fig. 8, are expected to increase our understanding, not only of frictional properties, but of dynamical properties of MEMS.

6. Summary

A method to measure friction between a micromachined gear and the hub on which it rotates has

been developed and implemented. Essential features of the method include: 1) the ability to determine experimentally the physical parameters necessary for the friction analysis, and 2) the ability to determine experimentally the frictional forces during normal operation. The physical parameters experimentally measured are consistent with those theoretically expected. *In-situ* measurements of an engine running at a speed of 18300 rpm reveal that conventional friction ($F_f = \mu F_n$; $\mu \sim 0.5$) occurs between the gear and hub for low applied forces. For drive signals that result in higher forces, the effective frictional force abruptly increases, indicating an abrupt change in the fundamental nature of the frictional forces between the gear and hub. In both cases, the frictional forces fluctuate as the gear rotates.

The method to make *in-situ* friction measurements of rotating structures has the potential to significantly improve the performance and reliability of MEMS devices. Increasing our fundamental understanding of friction in MEMS can lead to more robust designs and processes (including lubrication treatments). The method also makes possible the creation of engineered drive signals that reduce parasitic forces, thereby improving reliability and performance.

7. Acknowledgments

References

1. M. Mehregany, S. Senturia, and J. Lang, "Friction and wear in microfabricated harmonic side-drive motors", Solid-State Sensor and Actuator Workshop, June 4-7, 1990, Hilton Head Island, South Carolina, pp. 17-22

2. K. Deng, R. Collins, M. Mehregany, and C. Sukenik, "Performance impact of monolayer coating of polysilicon micromotors", J. Electrochem. Soc., Vol 142 (1995), pp. 1278-1285.

3. L. Fan, Y. Tai, and R. Muller, "IC-processed electrostatic micromotors", Sensors and Actuators, 20 (1989), pp. 41-47.

4. Y. Tai and R. Muller, "Frictional study of IC-processed micromotors", Sensors and Actuators, A21-A23 (1990), pp. 180-183.

5. Technology of the Year award, Industry Week, A Penton Publication, Vol 244, No. 23, Dec 18, 1995, pp. 30-34.

6. E. J. Garcia and J. J. Sniegowski, "Surface micromachined microengine", Sensors and Actuators A, Vol. 48, (1995) pp. 203-214.

7. J. J. Sniegowski and E. J. Garcia, "Microfabricated actuators and their application to optics", Proc. SPIE Miniaturized Systems with Micro-Optics and Micromechanics, Vol. 2383. San Jose, CA, Feb. 7-9, 1995, pp. 46-64.

8. W. C. Tang, Ph.D. Thesis, University of California, Berkeley, 1990.

9. Y. Cho, A. Pisano, and R. Howe, "Viscous damping model for laterally oscillating microstructures", J. Microelectromech. Syst., Vol. 3, (1994), pp. 81-87; D. W. Burns, Ph.D. Thesis, University of Wisconsin, Madison, 1988.

10. If the argument of the square root is positive, the voltage is applied to the comb pulling in the positive direction (see Fig. 2). If the argument of the square root is negative, the voltage is applied to the comb pulling in the negative direction (in this case, the absolute value is taken to evaluate the square root).

11. In the present context, ω is an arbitrary constant angular speed, and is conceptually different from the frequency associated with Eqs. (15) and (16), a natural frequency of the system.

12. When the gear is rotated to ~180°, the y-axis comb drive experiences its maximum displacement. At this position of maximum deflection, the lateral off-axis stiffness of the support springs is significantly reduced. This permits the y-axis comb drive to be electrostatically displaced in the x direction, where it laterally clamps to the alignment guides. This clamping impedes further rotation of the gear until the applied voltage drops below the de-clamping threshold. A design solution has been implemented that will mitigate this behavior.

13. J. Huang, Q. Tong, and P. Mao, "Gas-lubricated microbearings for microactuators", Sensors and Actuators A, 35 (1992), pp. 69-75.

DISCLAIMER